Langmuir
Article
pubs.acs.org/Langmuir

Highly Ductile Multilayered Films by Layer-by-Layer Assembly of Oppositely Charged Polyurethanes for Biomedical Applications†

Paul Podsiadlo,[‡] Ming Qin,[‡] Meghan Cuddihy,[‡] Jian Zhu,[‡] Kevin Critchley,[‡] Eugene Kheng,[§] Amit K. Kaushik,[§] Ying Qi,[#] Hyoung-Sug Kim,[¶,+] Si-Tae Noh,[¶] Ellen M. Arruda,[§,▽] Anthony M. Waas,[∥,§] and Nicholas A. Kotov*[,‡,⊥,#]

[‡]*Departments of Chemical Engineering and* [§]*Mechanical Engineering and* [∥]*Aerospace Engineering and* [⊥]*Biomedical Engineering and* [#]*Materials Science and Engineering and* [▽]*Program in Macromolecular Science and Engineering, University of Michigan, Ann Arbor, Michigan 48109,* [¶]*Department of Chemical Engineering, Hanyang University, Ansan 425-791, Kyounggi-Do, South Korea, and* [+]*R&D Center, Hepce Chemical Company, Ltd., Ansan 425-836, Kyounggi-Do, South Korea*

Received June 15, 2009. Revised Manuscript Received August 31, 2009

Multilayered thin films prepared with the layer-by-layer (LBL) assembly technique are typically "brittle" composites, while many applications such as flexible electronics or biomedical devices would greatly benefit from ductile, and tough nanostructured coatings. Here we present the preparation of highly ductile multilayered films via LBL assembly of oppositely charged polyurethanes. Free-standing films were found to be robust, strong, and tough with ultimate strains as high as 680% and toughness of ~30 MJ/m^3. These results are at least 2 orders of magnitude greater than most LBL materials presented until today. In addition to enhanced ductility, the films showed first-order biocompatibility with animal and human cells. Multilayered structures incorporating polyurethanes open up a new research avenue into the preparation of multifunctional nanostructured films with great potential in biomedical applications.

Introduction

Multilayered nanostructured thin films prepared with the layer-by-layer (LBL) assembly technique have gained wide popularity in the past decade.[1] Since its inception in the early 1990's, the LBL field has experienced rapid growth, and today it is being utilized for a wide variety of applications, ranging from nanocomposites,[2−4] drug delivery platforms,[5,6] superhydrophobic coatings,[7] fuel cell and photovoltaic membranes,[8] microbatteries,[9,10] and onto solid-state memory devices.[11] Overall, the technique has shown remarkable versatility in combining a variety of components into functional structures, including nanoparticles,[12−14] nanotubes and nanowires,[2,15,16] nanoplates,[3,4] dendrimers,[17] polysaccharides,[18] polypeptides and DNA,[19−21] proteins,[22] and viruses.[9,10,23,24]

Most of the LBL films presented until today can be considered in general as nonductile structures, while many applications, such as flexible electronics or biomedical coatings, would greatly benefit from enhanced ductility and toughness. In fact, nearly all LBL films show elastic moduli typically of a few gigapascals[2,3,25−29] (as high as 106 GPa[4]) and only a few percentiles of ultimate strain. Two recent examples of hydrated multilayers and LBL tubes were shown to be much "softer" in nature, with moduli of only tens to a few hundreds of megapascals; however, no strain data were provided.[30,31] In

† Part of the "Langmuir 25th Year: Self-assembled polyelectrolyte multilayers: structure and function" special issue.

*To whom correspondence should be addressed. Tel.: (734) 763-8768. Fax: (734) 764-7453. E-mail: kotov@umich.edu.

(1) Decher, G. *Science* **1997**, *277*, 1232.
(2) Mamedov, A. A.; Kotov, N. A.; Prato, M.; Guldi, D. M.; Wicksted, J. P.; Hirsch, A. *Nat. Mater.* **2002**, *1*, 190.
(3) Tang, Z. Y.; Kotov, N. A.; Magonov, S.; Ozturk, B. *Nat. Mater.* **2003**, *2*, 413.
(4) Podsiadlo, P.; Kaushik, A. K.; Arruda, E. M.; Waas, A. M.; Shim, B. S.; Xu, J. D.; Nandivada, H.; Pumplin, B. G.; Lahann, J.; Ramamoorthy, A.; Kotov, N. A. *Science* **2007**, *318*, 80.
(5) Wood, K. C.; Chuang, H. F.; Batten, R. D.; Lynn, D. M.; Hammond, P. T. *Proc. Natl. Acad. Sci. U.S.A.* **2006**, *103*, 10207.
(6) Wood, K. C.; Zacharia, N. S.; Schmidt, D. J.; Wrightman, S. N.; Andaya, B. J.; Hammond, P. T. *Proc. Natl. Acad. Sci. U.S.A.* **2008**, *105*, 2280.
(7) Zhai, L.; Cebeci, F. C.; Cohen, R. E.; Rubner, M. F. *Nano Lett.* **2004**, *4*, 1349.
(8) Tokuhisa, H.; Hammond, P. T. *Adv. Funct. Mater.* **2003**, *13*, 831.
(9) Nam, K. T.; Kim, D. W.; Yoo, P. J.; Chiang, C. Y.; Meethong, N.; Hammond, P. T.; Chiang, Y. M.; Belcher, A. M. *Science* **2006**, *312*, 885.
(10) Nam, K. T.; Wartena, R.; Yoo, P. J.; Liau, F. W.; Lee, Y. J.; Chiang, Y. M.; Hammond, P. T.; Belcher, A. M. *Proc. Natl. Acad. Sci. U.S.A.* **2008**, *105*, 17227.
(11) Lee, J. S.; Cho, J.; Lee, C.; Kim, I.; Park, J.; Kim, Y. M.; Shin, H.; Lee, J.; Caruso, F. *Nat. Nanotechnol.* **2007**, *2*, 790.
(12) Kotov, N. A.; Dekany, I.; Fendler, J. H. *J. Phys. Chem.* **1995**, *99*, 13065.
(13) Keller, S. W.; Kim, H. N.; Mallouk, T. E. *J. Am. Chem. Soc.* **1994**, *116*, 8817.
(14) Cooper, T. M.; Campbell, A. L.; Crane, R. L. *Langmuir* **1995**, *11*, 2713.
(15) Podsiadlo, P.; Choi, S. Y.; Shim, B.; Lee, J.; Cuddihy, M.; Kotov, N. A. *Biomacromolecules* **2005**, *6*, 2914.
(16) Podsiadlo, P.; Sui, L.; Elkasabi, Y.; Burgardt, P.; Lee, J.; Miryala, A.; Kusumaatmaja, W.; Carman, M. R.; Shtein, M.; Kieffer, J.; Lahann, J.; Kotov, N. A. *Langmuir* **2007**, *23*, 7901.
(17) He, J. A.; Valluzzi, R.; Yang, K.; Dolukhanyan, T.; Sung, C. M.; Kumar, J.; Tripathy, S. K.; Samuelson, L.; Balogh, L.; Tomalia, D. A. *Chem. Mater.* **1999**, *11*, 3268.
(18) Lvov, Y.; Onda, M.; Ariga, K.; Kunitake, T. *J. Biomater. Sci., Polym. Ed.* **1998**, *9*, 345.
(19) Richert, L.; Lavalle, P.; Vautier, D.; Senger, B.; Stoltz, J. F.; Schaaf, P.; Voegel, J. C.; Picart, C. *Biomacromolecules* **2002**, *3*, 1170.
(20) Boulmedais, F.; Ball, V.; Schwinte, P.; Frisch, B.; Schaaf, P.; Voegel, J. C. *Langmuir* **2003**, *19*, 440.
(21) Lvov, Y.; Decher, G.; Sukhorukov, G. *Macromolecules* **1993**, *26*, 5396.
(22) Lvov, Y.; Ariga, K.; Kunitake, T. *Chem. Lett.* **1994**, 2323.
(23) Yoo, P. J.; Nam, K. T.; Qi, J. F.; Lee, S. K.; Park, J.; Belcher, A. M.; Hammond, P. T. *Nat. Mater.* **2006**, *5*, 234.
(24) Tang, Z. Y.; Wang, Y.; Podsiadlo, P.; Kotov, N. A. *Adv. Mater.* **2006**, *18*, 3203.
(25) Jiang, C. Y.; Markutsya, S.; Pikus, Y.; Tsukruk, V. V. *Nat. Mater.* **2004**, *3*, 721.
(26) Ko, H.; Jiang, C. Y.; Shulha, H.; Tsukruk, V. V. *Chem. Mater.* **2005**, *17*, 2490.
(27) Gunawidjaja, R.; Jiang, C. Y.; Peleshanko, S.; Ornatska, M.; Singamaneni, S.; Tsukruk, V. V. *Adv. Funct. Mater.* **2006**, *16*, 2024.
(28) Lin, Y. H.; Jiang, C.; Xu, J.; Lin, Z. Q.; Tsukruk, V. V. *Adv. Mater.* **2007**, *19*, 3827.
(29) Nolte, A. J.; Rubner, M. F.; Cohen, R. E. *Macromolecules* **2005**, *38*, 5367.
(30) Schoeler, B.; Delorme, N.; Doench, I.; Sukhorukov, G. B.; Fery, A.; Glinel, K. *Biomacromolecules* **2006**, *7*, 2065.
(31) Cuenot, S.; Alem, H.; Louarn, G.; Demoustier-Champagne, S.; Jonas, A. M. *Eur. Phys. J. E* **2008**, *25*, 343.

another recent report, Hammond's group showed preparation of a film with unusually high ultimate strain. In this work, Lutkenhaus et al. showed that hydrogen bonded multilayers of poly(ethylene oxide) and poly(acrylic acid) can have tensile modulus (E) of 2 MPa and ultimate tensile strain (ε_{UTS}) of 360%.[32] The authors attributed this high ductility to lowered glass transition temperature and also hydration of the films.

In this paper we focus on the preparation of LBL composites using a new assembly component: water-soluble polyurethanes (PUs). PUs are well-known for their strength and toughness, and they have found broad applications in construction, transportation, household appliances, packaging, electronics, and implantable biomedical devices, to name a few. PUs also represent an important new component of LBL technique with a variety of potential research directions. To this end, recently we showed preparation of millimeter-thick composites by hierarchical stacking of "exponential" LBL films composed of cationic PU (Cat PU) and poly(acrylic acid).[33] Individual, ~70 μm-thick films showed ε_{UTS} of ~250%, ultimate tensile strength (σ_{UTS}) of ~30 MPa, and toughness (K) of ~50 MJ/m^3. Hierarchical stacking and consolidation of the films into >500 μm-thick structures, enhanced the ultimate strain to $\varepsilon_{UTS} \sim 360\%$, along with improvements in strength and toughness ($\sigma_{UTS} \sim 85$ MPa, $K \sim 130$ MJ/m^3).

Here, we demonstrate for the first time the preparation of highly ductile nanostructured films from LBL assembly of oppositely charged PUs. Film buildup was characterized with ultraviolet−visible (UV−vis) spectroscopy and ellipsometry, revealing uniform and steady growth. Composition of the film was characterized with X-ray photoelectron spectroscopy (XPS) and elemental analysis, revealing an overall intermediate composition between the two components and anisotropic distribution between Cat PU- and anionic PU (An PU)-terminated surfaces, as was expected from alternating deposition of polymer layers. Internal structure was characterized with scanning electron microscopy (SEM) and phase-contrast atomic force microscopy (AFM). SEM of a cross-section revealed layered architecture, while AFM showed cellular organization of the hard and soft domains on the surface of the LBL film. Furthermore, we show preparation of free-standing films and the results from evaluation of their mechanical properties. The LBL films were found to be highly robust and ductile with ultimate strains reaching as high as $\varepsilon_{UTS} \sim 680\%$. This result is more than 2 orders of magnitude greater than most LBL assemblies prepared thus far. In addition to ductility, we have also evaluated the biocompatibility of the films with rat skin and human osteoblast cell lines. We found that both cell types were highly compatible with the surfaces as indicated by live−dead assays and quantification of double-stranded DNA (dsDNA). The relative ease of tuning the chemical composition and thus mechanical properties of the PUs opens up new possibilities for the preparation of highly ductile and multifunctional nanostructured films for biomedical applications.

2. Experimental Procedure

Materials and LBL Assembly. Aqueous dispersions of the cationic (Cat PU, ~35 wt %, MW ≈ 92 000) and anionic (An PU, ~35 wt %, MW ≈ 280 000) PUs were obtained from Hepce Chem. Co., South Korea, and used as received. Solutions used in the LBL assembly were diluted to ~3.5 wt % concentrations. The pH values of the resulting solutions were pH ≈ 7.7 and pH ≈ 9.1, for Cat PU and An PU, respectively. The LBL assembly was performed on microscope glass slides and silicon wafers either by hand for initial characterization or using a StratoSequence IV automated dipping robot, from nanoStrata, Inc. (Tallahassee, FL). LBL films used for cell culture experiments were assembled on glass slides prescored into 1 cm × 1 cm squares for standardization and easy fitting into 24-cell culture well-plates. Upon deposition, glass slides were broken up into pieces and used for further experiments. The films were assembled using 2 min dips into the PU solutions followed by 2−1 min rinses with pure deionized (DI) water and a single, 1 min drying with compressed air. Free-standing films consisting of 300 bilayers were isolated by etching of the glass slides with 1% hydrofluoric acid. After thorough rinsing with pure water, the films were dried in an oven at 80 °C. Pure PU films were prepared by dry-casting of the diluted solutions.

Mechanical Property Evaluation. The films were subjected to uniaxial tensile tests using a vertical stretcher from Test Resources. The tests were performed under ambient conditions (~35% relative humidity). Dog bone shaped test specimens were lightly airbrushed with a random, black speckle pattern before being cut with an elliptical punch to a gauge length of 13 mm and a width of 2−3 mm. The specimens were pulled apart at a displacement rate of 80 μm/s, and images of the center gage section were collected every 5 s, using a Nikon D2x camera equipped with a 300 mm macro lens. The reactive tensile load on the specimen was measured using a 111 N load cell. The collected speckle images were analyzed using ImageJ software equipped with a MetaJ tracking macro. The X and Y coordinate data of two neighboring speckles, as a function of specimen load, was then processed with a MATLAB script to produce Green−Lagrange strain data corresponding to each load state. The Green−Lagrange strain E_{11} in the direction of the axial force is defined as $E_{11} = (1/2)*[(1 + e_1)^2 - 1]$, where $e_1 = (dx - dX)/dX$, is the change in length per unit length of a line element that is initially parallel to the direction of axial stretching.[34] The force measurements from the load cell were divided by the measured initial thickness and initial width of the sample gage section to give engineering stress. This procedure results in a plot of engineering stress versus e_1. Three to five tests were performed for each material type.

Film-Structure Characterization. The LBL process was monitored using an 8453 UV−vis Chem Station spectrophotometer (Agilent Technologies), with data collected after each deposited layer. The reference spectrum for the instrument was ambient air, and collected spectra of the adsorbed material were compared to UV−vis absorbance of a fresh, piranha-cleaned glass slide. SEM images were obtained with an FEI Nova Nanolab dual-beam FIB and scanning electron microscope operated at 15 kV beam voltage. Ellipsometry measurements were obtained using a BASE-160 Spectroscopic Ellipsometer (J. A. Woollam Co., Inc.). The instrument was calibrated to a standard silicon wafer with a thin layer of silicon dioxide, and the subsequent calculations were fitted using a Cauchy's model. AFM experiments were performed in tapping mode using NanoScope IIIa (Veeco Instruments, Santa Barbara, CA). Differential scanning calorimetry (DSC) analysis was performed using a Perkin-Elmer DSC-7 (PerkinElmer, Wellesley, MA). A small amount (5 mg) of the sample was encapsulated in an aluminum pan and was first heated from 10 to 300 °C at a scan rate of 10 °C/min. The sample was then cooled from 300 to 10 °C at the same rate. Data acquisition and processing was done with PerkinElmer Pyris software. X-ray powder diffraction (XRD) patterns were collected on a Rigaku Miniflex (Rigaku, The Woodlands, TX). The diffractometer is equipped with a Cu X-ray tube (Cu Kα, λ = 1.54059 Å) with an operating voltage of 30 kV and current of 15 mA. Scans were performed continuously from 2° to 90° 2θ

(32) Lutkenhaus, J. L.; Hrabak, K. D.; McEnnis, K.; Hammond, P. T. *J. Am. Chem. Soc.* **2005**, *127*, 17228.

(33) Podsiadlo, P.; Arruda, E. M.; Kheng, E.; Waas, A. M.; Lee, J.; Critchley, K.; Qin, M.; Chuang, E.; Kaushik, A. K.; Kim, H. S.; Qi, Y.; Noh, S. T.; Kotov, N. A. *ACS Nano* **2009**, *3*, 1564.

(34) Malvern, L. *An Introduction to the Mechanics of a Continuous Medium*; Prentice-Hall: Upper Saddle River, NJ, 1969.

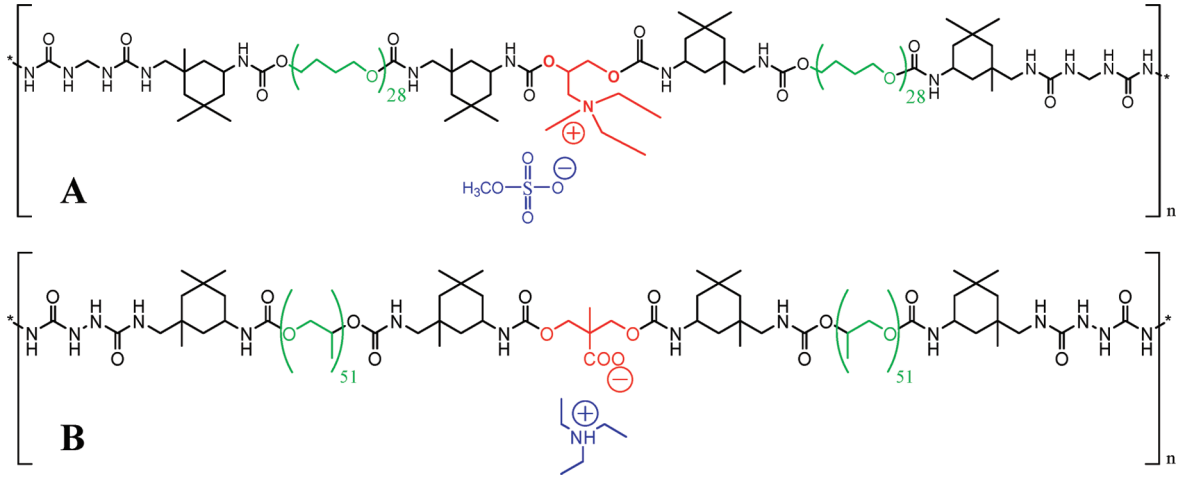

Figure 1. Chemical structures of (A) Cat and (B) An PUs. Charged groups are highlighted in red, counterions in blue, and soft segments in green.

in increments of 5° per min. Elemental analysis was performed using a Perkin-Elmer 2400 Series II combustion analyzer.

Composition Analysis by XPS. XPS spectra were obtained using a Thermo Electron Corporation ESCA Lab 250 with a chamber pressure maintained below 5×10^{-9} mbar during acquisition. A monochromated Al Kα X-ray source (15 kV; 150 W) irradiated the samples, with a spot diameter of approximately 0.5 mm. The spectrometer was operated in Large Area XL magnetic lens mode using pass energy of 150 and 20 eV for survey and detailed scans, respectively. The spectra were obtained with an electron takeoff angle of 90°. High-resolution spectra were fitted using Avantage (Thermo VG software package) peak fitting algorithms. All spectra have been normalized to the C 1s peak (284.6 eV).

Cell Culture. Human osteoblast cell line hFOB 1.19 (CRL-11372) and *Rattus norvegicus* (FR) rat skin cell line were purchased from American Tissue Culture Corporation (ATCC, Manassas, VA) and grown as recommended by ATCC. Specifically, hFOB 1.19 cells were grown in 45% Ham′s F12 medium, 45% Dulbecco's modified Eagle's medium (DMEM) and 10% fetal bovine serum (Gibco, Frederick, MD) supplemented with 0.3 mg/mL G-418 (Gibco, Frederick, MD). FR cells were grown in Eagle's minimum essential medium (EMEM) supplemented with 10% fetal bovine serum and 1% penicillin streptomycin. Cells were grown at 37 °C and 5% CO_2, while changing medium every 2−3 days.

Cell Loading and Culture on Films. For each film-bilayer-number (0.5, 1, 10, 10.5), 24 pieces of film on cut glass slides were placed individually into wells of 12-well microplates. Films were sterilized in 70% ethanol for 30 min and rinsed three times with phosphate buffered saline (PBS). Twelve of the films were slated for FR culture, and the remaining 12 were slated for hFOB culture. For each cell type, an equal number of cells were placed onto the films, and all wells were filled with respective media and incubated. The media was changed every 2−3 days.

At two, five, and seven days, the following procedure was performed to prepare cells for dsDNA quantification. Media was removed from the wells of three films for each cell type and bilayer number, and films were rinsed in PBS. Films were then removed from wells and placed into new wells to be treated with trypsin−ethylenediaminetetraacetic acid (EDTA) until cells detached from the films. After detachment, cells were collected with trypsin−EDTA into microcentrifuge tubes, and films were rinsed once more in PBS that was added to the cell collection tubes and stored at −70 °C so that all samples could be analyzed at once.

Optical and Confocal Microscopy for Viability. After three days of culture, one film of each cell type and bilayer number was rinsed with PBS and stained with 2 μM calcein AM and 4 μM EthD-1 using a Live/Dead Viability/Cytotoxicity Kit (Invitrogen Corporation, Carlsbad, CA) for 30 min. Samples were rinsed again and viewed immediately using a Leica TCS SP2 Confocal Laser Scanning Microscope with 10× and 20× objectives.

To further examine morphology of cells on films, after 4 days of culture, cells were imaged directly on films in wells using a Nikon (Melville, NY) Eclipse TS100 inverted microscope and a Qimaging (Surrey, BC) Micropublisher 3.3 RTV camera.

dsDNA Quantification. At the time of dsDNA quantification, all cell collections were thawed and centrifuged for 5 min at 300 × *g*. Excess trypsin−EDTA and PBS were removed, and cells were resuspended and sonicated in 500 μL passive lysis buffer (Promega Corporation, Madison, WI). Samples were then centrifuged for 10 min at 10 000 rpm. Of the supernatant, 50 μL was prepared for dsDNA quantification using Quant-iT PicoGreen dsDNA Reagent (Invitrogen Corporation, Carlsbad, CA), according to manufacturer protocol. Sample fluorescence was measured at 520 nm by excitation at 480 nm on a Biotek Synergy 2 Multi-Detection Microplate Reader (Winooski, VT).

3. Results and Discussion

A. Assembly and Structure. PUs represent a very large family of polymers, with a common structural feature being the urethane linkers connecting its subunits. In this work we used two commercially available PUs with chemical compositions shown in Figure 1. We note that the particular compositions are by no means the only available; however, they satisfy two important parameters for LBL assembly: (1) they are soluble in aqueous conditions as the result of a high density of hydrophilic groups and (2) they have charged units (Figure 1, red groups) in the form of a short tertiary ammonium side chain in the Cat PU and a carboxylic acid group in the An PU. Furthermore, we chose these particular structures because of their fairly long "soft" segments (Figure 1, green groups), $(-CH_2-CH_2-CH_2-CH_2-O-)_{28}$ and $(-C_2H_4-CH_2-O-)_{51}$, for Cat and An PUs, respectively, which impart these polymers with high ductility at the molecular and nanoscale levels.

In a typical assembly, piranha-cleaned substrates (microscope glass slides or silicon wafers) were first immersed into a ∼3.5 wt % solution of Cat PU for 2 min, rinsed with DI water, and dried with compressed air. In this stage, Cat PU adsorbs onto the charged substrate via electrostatic and hydrogen bonds and, under optimal conditions, reverses surface charge to accommodate adsorption of a negative species. After adsorption of the polycation, the substrates were immersed into a ∼3.5 wt % solution of An PU for

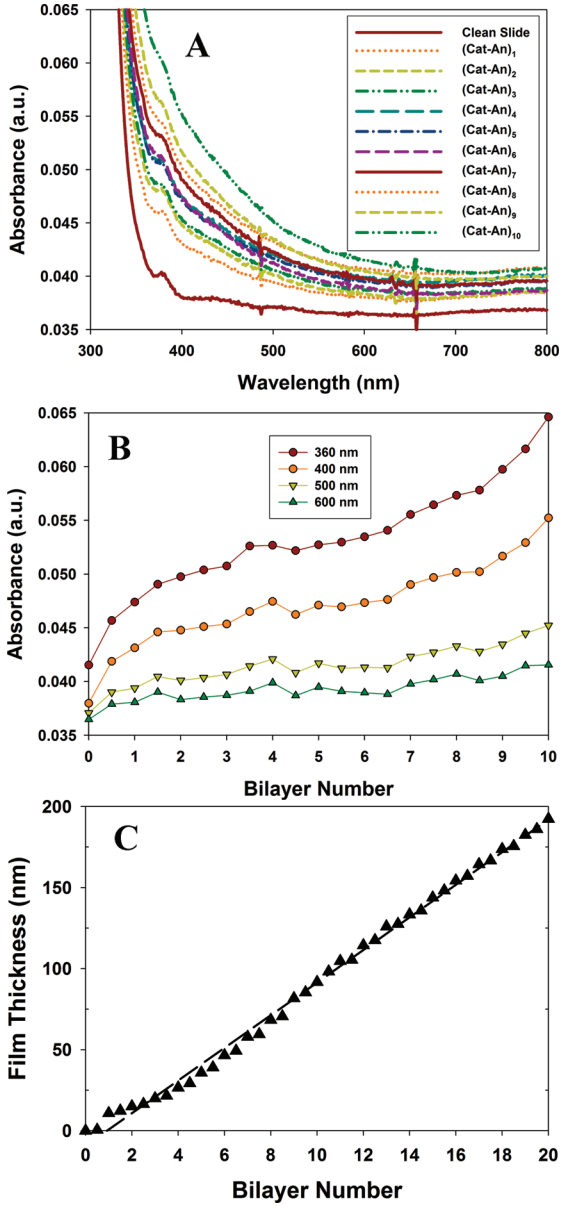

Figure 2. (A) Compilation of UV−vis absorbance spectra for Cat PU−An PU assembly for the first 10 bilayers. (B) Absorbance versus bilayer number regressions for Cat PU−An PU assembly from panel A showing uniform growth. (C) Ellipsometry results for Cat PU−An PU assembly on silicon substrate.

2 min, and again rinsed with DI water, and dried with compressed air. Similarly to the polycation adsorption, the adsorbing polyanion reverses the surface charge to negative and returns the substrate to the original state. At this stage, the substrate is covered with a pair of cationic and anionic layers, which from this point forward will be referred to as bilayers. Reversal of the surface charge to the starting point allowed for adsorption of new bilayers allowing incremental growth of the multilayers to a desired final thickness.

Film buildup was characterized with UV−vis spectroscopy and ellipsometry. (Figure 2) Figure 2A shows compilation of spectra collected after successive adsorption of (Cat PU−An PU)$_1$ bilayers up to a total of 10 bilayers, denoted as (Cat PU−An PU)$_{10}$. Similarly to previous demonstrations of multilayer buildup, the assembly conditions described above showed uniform and regular growth. Plotting of absorbance versus bilayer number for different wavelengths of light (Figure 2B) revealed steady and

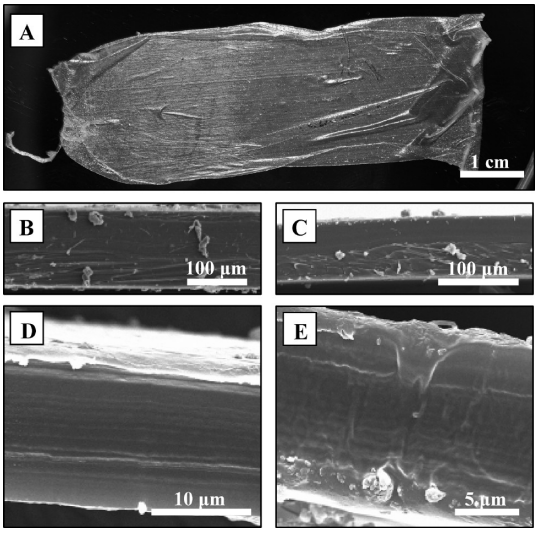

Figure 3. (A) Photograph of a free-standing, 300-bilayer Cat PU−An PU LBL film. (B) SEM cross-section of pure Cat PU. (C) SEM cross-section of pure An PU. (D,E) Cross-sectional SEM images of the free-standing, 300-bilayer Cat PU−An PU LBL film showing regular stratification. All films were cut with a razor blade to reveal the cross-section.

nearly linear growth with some evidence of an upswing when 10 bilayers were approached. Interestingly, ellipsometry showed complete linearity up to 20 bilayers with incremental growth of nearly ~10 nm per bilayers. (Figure 2C).

Having established successful growth of the multilayer, we proceeded with growing thick films on microscope glass slides using automatic dipping robots from NanoStrata (Tallahassee, FL). A set of 300-bilayer films was prepared, and free-standing films were separated using the substrate etching with HF solution described in our previous publications[3] (Figure 3A). Compared to the previous publications, we allowed the detached film to float in pure DI water to remove any excess of HF. The films were then lifted out from water using a rigid Teflon substrate.

Upon removal from water, films supported on the Teflon substrate were placed in a convection oven at 80 °C and allowed to dry. Using Teflon allowed for easy detachment of free-standing films. The films were found to be thin, highly robust, and ductile. Careful handling was required as the films showed substantially lower stiffness when compared to the films incorporating nanoparticles.[2−4]

SEM characterization of the free-standing films revealed uniform cross-section however with much greater thickness than expected. Extrapolation of the data obtained from ellipsometry suggested that the thickness should not be more then ~3 μm for the 300-bilayer film, while the SEM revealed approximately 4x greater thickness of ~13 μm. This translates into an average of ~40 nm per bilayer. This could potentially be a result of incomplete rinsing of the films; however, a closer look at the SEM images revealed a well-defined stratified structure throughout the entire thickness which was not observed in the pure polymers. (Figures 3B − 3E) An explanation may come from the fact that the charge density along the polymers' backbones is small and it is already well established that weakly charged polyelectrolytes can have nonlinear and even exponential growth leading to structures having thicknesses in excess of 100 μm for 200 bilayers.[33,35,36]

(35) Podsiadlo, P.; Michel, M.; Lee, J.; Verploegen, E.; Kam, N. W. S.; Ball, V.; Qi, Y.; Hart, A. J.; Hammond, P. T.; Kotov, N. A. *Nano Lett.* **2008**, *8*, 1762.
(36) Picart, C.; Mutterer, J.; Richert, L.; Luo, Y.; Prestwich, G. D.; Schaaf, P.; Voegel, J. C.; Lavalle, P. *Proc. Natl. Acad. Sci. U.S.A.* **2002**, *99*, 12531.

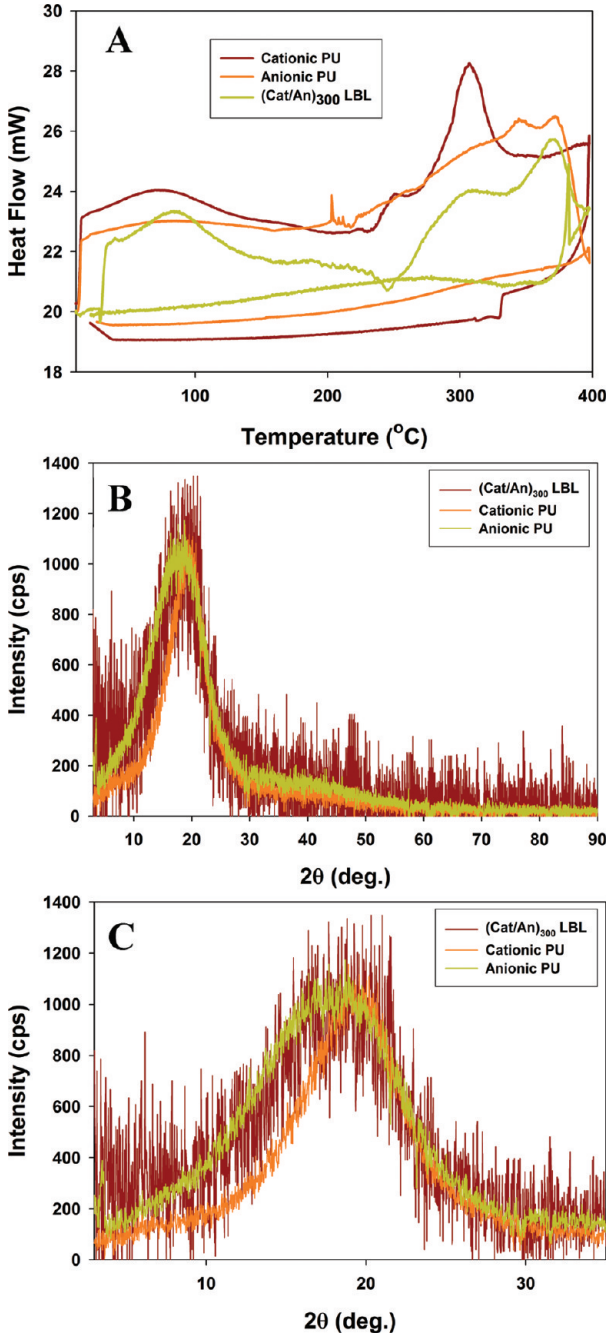

Figure 4. (A) DSC spectra comparison for pure polymers and LBL film. (B,C) WAXS spectra comparison of pure polymers and LBL film. The spectra in DSC and WAXS are normalized to the same height due to large differences in the thickness of the samples. Because of small thickness of the LBL film, the spectrum shows lower signal-to-noise ratio when compared to that of pure polymers.

An important question that one needs to ask is how the molecular and nanoscale organization of the polymers is affected by nanostructuring via alternating layering of nanometer-thick strata in LBL. This is an especially important question because the exceptional ductility of the PUs is attributed to the ability of formation of "hard" (crystalline) and "soft" (amorphous) domains. In the case of our polymers, the hard domains contain charged groups, which are primarily responsible for the formation of electrostatic interactions between each other and may compromise the ability of the two polymers to form ductile material. To help answer this question, we characterized the chemical composition of the LBL film using elemental analysis and XPS.

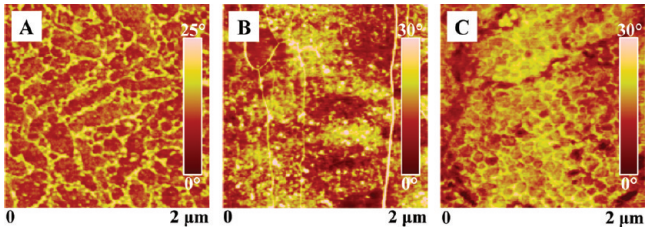

Figure 5. Phase-contrast AFM images of surface morphologies for (A) Cat PU, (B) An PU, and (C) Cat PU−An PU LBL film.

(see the Experimental Section and the Supporting Information) The XPS results revealed substantial differences in composition between Cat- and An-PU-terminated surfaces. The Cat-PU-terminated surface had a ~1:2 molar ratio (~1:1.5 wt % ratio) of the An PU to Cat PU monomers, while the An-PU-terminated surface had ~2.6:1 (~3.5:1 wt % ratio) An PU to Cat PU monomers. Because of the close similarity between the two polymers, it was difficult to accurately characterize the composition of the LBL films using elemental analysis; however, we could conclude that the film does not have a preferential composition of either of the two polymers. DSC characterization of the pure polymers and the LBL film (Figure 4A) showed that the characteristic transition peak of Cat PU present at ~300 °C was greatly suppressed when compared to the peak of An PU at ~375 °C. Furthermore, characterization of the polymers and LBL film by wide-angle X-ray scattering (WAXS) showed that the multilayer film in fact contains amorphous domains characteristic to both components, spanning a 2θ angle range of approximately 15° (from 10° to 25°). (Figure 4B,C) Overall, we can conclude that the LBL film has close to equal molar concentration of the two PUs, with slightly greater content of the An PU.

AFM characterization of top surface morphologies with phase contrast imaging mode showed striking differences between the different films. (Figure 5) First, the two oppositely charged PUs showed very different morphologies: Cat PU (Figure 5A) showed a distinctly granular structure with hard domains clearly contrasting the soft regions, while An PU showed very little contrast between the hard and soft domains. The hard domains in Cat PU have mainly oval shapes with widths up to ~150 nm and lengths as large as 2 μm (typical lengths are less than 1 μm). The LBL film also showed evidence of hard and soft domains as in the Cat PU (Figure 5C), but with very different morphology. The hard domains appear to form a cellular structure with hard domains having spherical shape and diameters up to ~150 nm. Overall, evidence of domain formation was encouraging for the ultimate goal of this work, i.e, preparation of ductile multilayered films.

B. Mechanical Properties. Evaluation of tensile mechanical properties of the films showed high ductility with properties being intermediate between the two components. (Figure 6 and Table 1) The Cat PU showed yield strength (σ_Y) of ~2 MPa, ultimate strength (σ_{UTS}) of ~30 MPa, modulus (E) of ~26 MPa, and ultimate tensile strain (ε_{UTS}) of ~540%. The An PU showed no evidence of yield strength, lower σ_{UTS} (~10 MPa) and E (~2 MPa); however, it showed much higher strain: ε_{UTS} ~ 1200%. Comparing to the two, the LBL film showed improvement in σ_Y to ~3 MPa, but significant reduction of σ_{UTS} to ~6.5 MPa. The modulus and strain showed intermediate values between the two polymers: E ~ 15 MPa and ε_{UTS} ~ 630%. The significant reduction in σ_{UTS} may be explained with fragility of the films to handling. While not visible with the naked eye, very soft nature of the

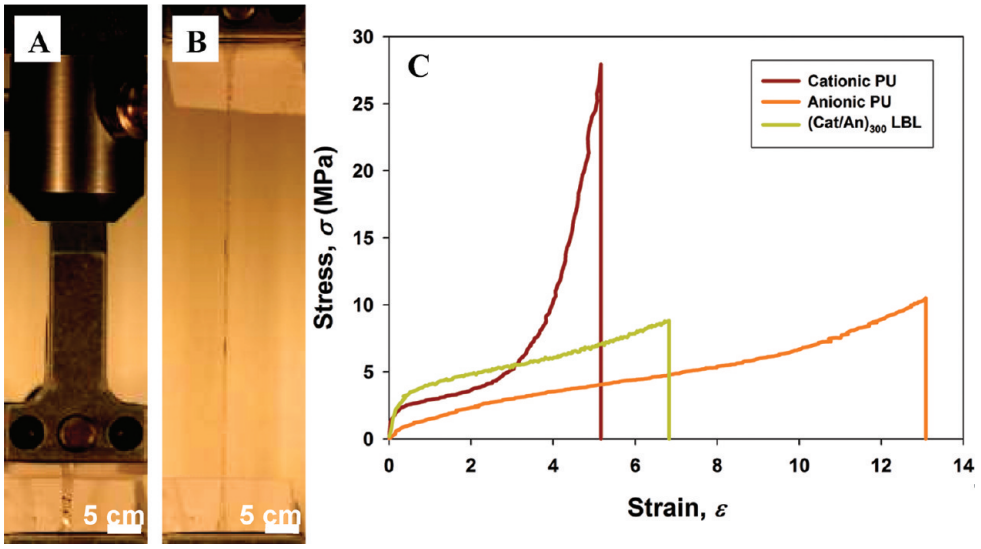

Figure 6. Mechanical properties of PUs and LBL film. (A,B) Photographs of a dog-bone specimen of a 300-bilayer LBL at $\varepsilon = 0$ and $\varepsilon \sim \varepsilon_{UTS}$ (prior to rupture), respectively. (C) Comparison of stress−strain responses for pure polymers and the LBL film.

Table 1. Experimental Results from Comparison of the Mechanical Properties of Cationic, Anionic, and Cat PU−An PU LBL Films

sample type	yield strength, σ_Y (MPa)	ultimate tensile strength, σ_{UTS} (MPa)	Young's modulus, E (MPa)	ultimate tensile strain, ε_{UTS} (%)	toughness, K (MJ/m^3)
Cat PU	2.3 ± 0.7	29 ± 2	26 ± 15	540 ± 40	43 ± 4
An PU		10 ± 1	2.4 ± 0.6	1220 ± 100	55 ± 9
Cat−An LBL	3.1 ± 0.4	6.5 ± 1.7	15 ± 6	630 ± 50	29 ± 8

films can be easily prone to defects from handling, and the ultimate strength and strain can be reduced by premature failure.

Furthermore, the improvement in σ_Y can be attributed to the formation of electrostatic cross-links between the two polymers. The same cross-links can also be responsible for decreasing the ultimate strain to values closer to those of the Cat PU. Overall, these are excellent results given that most of the previously reported LBL films showed 2 orders of magnitude lower strains.[2−4,35,37−39] They open new opportunities for research and applications, especially when the assemblies will be combined with different nanomaterials for preparation of mechanically responsive and ductile nanostructured assemblies.

C. Cell Culture Evaluation. The attachment and proliferation of cells can be controlled by various materials' surface properties, such as hydrophobicity, charge, chemistry, crystallinity, and topography. In particular, substrate surface charge can be manipulated to affect cell adhesion depending on cell type or the presence or absence of serum. Here, we utilized the simplicity of imposing a positive or negative charge on PU bilayer films to explore the biocompatibility of films of either charge. In this study, four-film-bilayer numbers were studied: 0.5, 1, 10, and 10.5. These were constructed in a manner such that Cat PU was the first bilayer applied, followed by An PU, such that 0.5 and 10.5 bilayer films presented a positively charged surface, while 1 and 10 bilayer films presented An PU on the surface.

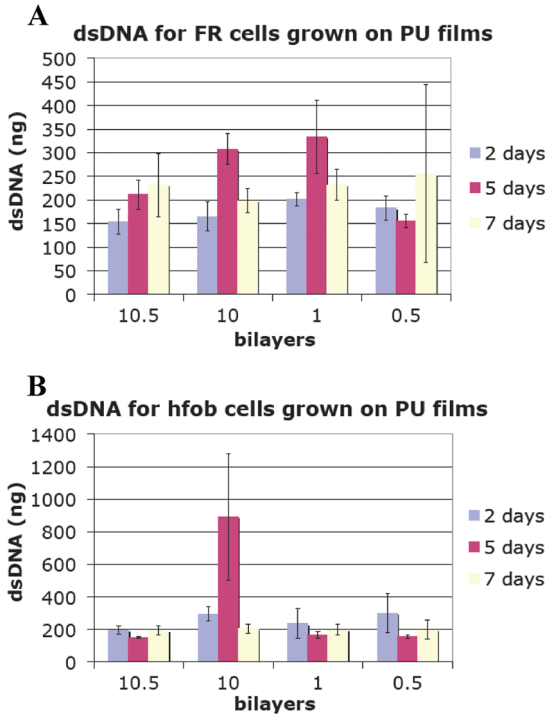

Figure 7. dsDNA data for (A) FR and (B) hFOB 1.19 cells at 2, 5, and 7 days for different numbers of bilayers. All samples appeared to maintain an approximately constant amount of cells present over the time studied.

We have evaluated biocompatibility of the different surfaces against 2 different cell lines: human osteoblasts (hFOB 1.19) and rat skin cells (FR). Both FR and hFOB 1.19 cell types were studied to explore the biocompatibility on PU films of skin and

(37) Gao, C. Y.; Leporatti, S.; Moya, S.; Donath, E.; Mohwald, H. *Langmuir* **2001**, *17*, 3491.
(38) Mertz, D.; Hemmerle, J.; Mutterer, J.; Ollivier, S.; Voegel, J. C.; Schaaf, P.; Lavalle, P. *Nano Lett*. **2007**, *7*, 657.
(39) Podsiadlo, P.; Liu, Z. Q.; Paterson, D.; Messersmith, P. B.; Kotov, N. A. *Adv. Mater*. **2007**, *19*, 949.

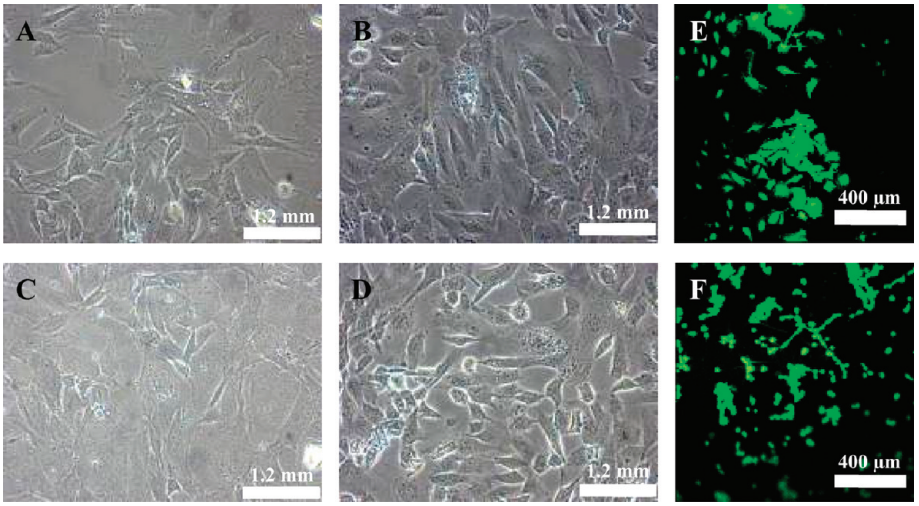

Figure 8. Inverted microscope images of (A,C) FR cells and (B,D) hFOB 1.19 cells on (A) 0.5, (B) 1.0, (C) 10, and (D) 10.5 bilayer films after 4 days of culture. (E,F) Representative images of live/dead assay after 3 days of culture. (E) FR cells on films with 1 bilayer. (F) hFOB 1.19 cells on films with 10 bilayers. Only live cells (green) are visible because the dead cells (red) typically detached from the substrates and were washed out with the cell culture serum.

bone cells of multiple species. The method in which biocompatibility was quantified was by assaying the amount of dsDNA present in a sample over the course of a week (Figure 7); comparing the amount of dsDNA in a set of samples is representative of number of cells in those samples. Here, it was observed that, for both cell types, the amount of cells present was fairly consistent with time. One could speculate that FR cells may be affected by the surface charge of the substrate, in that there is a trend toward growth over time for samples with 0.5 and 10.5 bilayers, whereas cell numbers remained fairly consistent for samples with 1 and 10 bilayers. This would indicate that perhaps for anionic charged surfaces, FR cells attach quickly and reach confluence, whereas for cationic charged surfaces initial attachment is limited, thus there is room for cells to replicate with time. In contrast, hFOB 1.19 samples have fewer trends over time, so these cells may attach and become confluent with equal time. One must also note that all cultures were performed with FBS, so one must consider cell adhesion to proteins in the serum that may adhere to the surfaces. These speculations must be supported with further data.

Both inverted microscope and confocal images of live/dead stained cells (Figure 8) demonstrate biocompatibility with all surfaces. In both sets of images, cells are spread and plentiful, indicating that cellular interactions with surfaces are attractive and biocompatible.

4. Conclusions

In conclusion, we presented here preparation and characterization of highly ductile free-standing LBL films. The films showed ultimate strains of several hundred percent, which are at least 2 orders of magnitude greater than most of previous LBL assemblies. A new assembly component, i.e., charged PUs, was instrumental to this demonstration, and this work represents the first use of PUs in multilayered assemblies. PUs constitute a large family of polymers with a wide range of compositions and, when combined with the wide array of already available assembly components, they represent a fundamentally novel material. In particular, the LBL films from PUs might be useful for biomedical applications as permanent implants such as artificial cartilage. Unlike standard PU blends, the LBL multilayers offer the possibility of producing nano/micro scale gradient structures with excellent control of the progression of mechanical properties, which is a common need for long-term implants.

Acknowledgment. The authors thank the U.S. Office of Naval Research (N00014-06-1-0473) for financial support. N.A.K. thanks AFOSR, NSF, DARPA, and NRL for the support of this research. P.P. thanks the Fannie and John Hertz Foundation for support of his work through a graduate fellowship. K.C. thanks the European Union under a Marie Curie Outgoing International Fellowship [MOIF-CT-2006-039636] for financial support. The authors acknowledge the staff of the Electron Microscopy Analysis Laboratory (University of Michigan) and their sponsor, the National Science Foundation (NSF) through Grant #DMR-0320740. We also acknowledge the receipt of NSF Grant #DMR-0420785 which enabled us to perform XPS.

Supporting Information Available: Detailed XPS compositional characterization of film surface and elemental analysis results. This material is available free of charge via the Internet at http://pubs.acs.org.